Polar Meteorol. Glaciol., **16**, 15–31, 2002

Sea ice thickness estimated from passive microwave radiometers

Kazutaka Tateyama[1], Hiroyuki Enomoto[2,3], Takenobu Toyota[4] and Shotaro Uto[5]

[1] *Sea Ice Research Laboratory, Institute of Low Temperature Science, Hokkaido University, 6–4–10, Minamigaoka, Mombetsu 094-0013*
[2] *Department of Civil Engineering, Kitami Institute of Technology, 165, Koen-cho, Kitami 090-8507*
[3] *Frontier Observational Research System for Global Change, 3173–25, Showa-machi, Kanazawa-ku, Yokohama 236-0001*
[4] *Institute of Low Temperature Science, Hokkaido University, Kita-19, Nishi-8, Kita-ku, Sapporo 060-0819*
[5] *National Maritime Research Institute, 6–38–1, Shinkawa, Mitaka-shi, Tokyo 181-0004*

Abstract: This study presents the findings of research into the correlation between sea ice thickness and passive microwave radiation. *In-situ* sea ice thickness samples were obtained from video observations by the icebreaker *Soya* during 1996–1998 and surface feature observations in 1997 by the visible and near-infrared radiometer AVNIR mounted on the ADEOS satellite. These sea ice thickness data were binned into grid cell data of the satellite microwave radiometer SSM/I for the same location, and averaged to provide an average ice thickness for a grid cell.

In order to survey the relationship between sea ice thickness and microwave radiation, two sea ice classification parameters for SSM/I were investigated as to their ability to estimate sea ice thickness. One sea ice classification parameter is the Polarization Ratio (PR), which was developed for a seasonally ice covered area and can distinguish three ice types: new ice, young ice, and first-year ice. Another parameter is the ratio between 37 GHz vertical polarization and 85 GHz vertical polarization ($R_{37V/85V}$). It can distinguish fast ice in addition to the three ice types that can be distinguished by the PR. These parameters showed correlation coefficients with *in-situ* sea ice thickness, -0.77 and 0.67, respectively, in this study. Estimated sea ice thickness derived from multiple regression analysis using PR and $R_{37V/85V}$ showed good correlation ($R=0.81$) with *in-situ* sea ice thickness.

1. Introduction

Arctic warming and the resulting decrease in the extent of sea ice has become one of the most important features of present global climate change. Warming events in polar and sub-polar regions affect not only sea ice coverage but also sea ice thickness. Thinning of the Arctic sea ice cover since the 1990s has been reported from submarine observations in the Scientific Ice Expeditions program (SCICEX) by Rothrock *et al.* (1999). To measure sea ice thickness, it is necessary to use a drill, sonar (Wadhams *et al*., 1991; Wadhams, 1997; Rothrock *et al*., 1999), a laser altimeter (Multala *et al*., 1996; Ishizu *et al*., 1999), or an electromagnetic inductance device (Haas *et al*., 1997). These methods observe sea ice thickness at a point or along a ship route, so coverage is limited. On the other hand, sea ice measurement by using satellite microwave remote

sensing provides area/macro sea ice information and has advantages such as availability of past data (since the 1970s), daily global observations and all weather operation.

The daily global sea ice monitoring mainly depends on data observed by passive microwave radiometers (Wensnahan *et al*., 1993). Some algorithms for qualitative estimation of sea ice thickness, in other words, sea ice type classification for the seasonal ice covered area by passive microwave sensors, have been exploited (Wensnahan *et al*., 1993; Cavalieri, 1994; Comiso, 1995; Tateyama *et al*., 2000). While passive microwave measurements of artificial thin (<6 cm) sea ice growth in a cold laboratory were carried out and it has been shown that the brightness temperature will commonly increase with ice growth (Grenfell and Comiso, 1986; Eppler *et al*., 1992; Wensnahan *et al*., 1993), these results were proved only in case of newly formed ice. Quantitative measurements of thick ice over 10 cm by passive microwave instruments have not been reported, although some papers have shown qualitatively that the brightness temperature increases with ice growth between new ice and first-year ice and decreases with growth of ice beyond the first year ice (Grenfell *et al*., 1992; Wensnahan *et al*., 1993; Cavalieri, 1994; Comiso, 1995; Nakayama *et al*., 2000). Thus, quantitative estimation techniques of sea ice thickness by satellite sensors have not been developed yet.

This study presents results of an attempt to estimate sea ice thickness using two ice classification parameters, based on microwave polarization and spectral gradient information from the satellite passive microwave instrument. These parameters were validated with *in-situ* sea ice thickness data taken by video observations from an icebreaker in the southernmost Sea of Okhotsk during Februaries 1996–1998. For this study, data of newly formed ice below 10 cm thickness were obtained from satellite visible and near-infrared images for January–March 1997. Accurate estimation of sea ice thickness from satellite data is difficult. Therefore we investigated carefully the inherent problems, bias and limitation of *in-situ* ice thickness data and satellite data for developing the sea ice thickness estimation method, and verified objectively the value of these data.

2. Data

2.1. Validation data

2.1.1. *In-situ* ice thickness data

Field and satellite observations were carried out in the southern Sea of Okhotsk during winters from 1996 to 1998 and are summarized in Table 1. Figure 1a shows the general location of the Sea of Okhotsk and our study area. *In-situ* ice thickness data were derived from the observations by Japan Coast Guard icebreaker *Soya* during the Februaries of 1996–1998 in the southernmost Sea of Okhotsk as shown in Fig. 1b. The National Maritime Research Institute (NMRI) had started video observation in 1991 and has continued in cooperation with the Institute of Low Temperature Science (ILTS), Hokkaido University, since 1996. These observations differ in time periods as noted in Table 1, and in their targets. While the NMRI observed ice thicknesses and positions at the end of February, Hokkaido University conducted observations at the beginning of February, and investigated not only ice thickness and position, but also ice concentration, surface albedo, snow depth and ice fabric (Toyota *et al*., 1999; Ukita *et*

al., 2000). Both the NMRI and ILTS monitored sea ice thickness by a downward-looking video camera mounted at the side deck of the ship and measured manually on a video image when the sides of broken ice floes were visible. The reading error in

Table 1. Summary of sea ice thickness observations by ship and using visible and microwave satellite instruments during 1996–1998.

Data	1996	1997	1998
Ship observations	NMRI: Feb. 23–28 ILTS: Feb. 3–5	NMRI: Feb. 27–29 ILTS: Feb. 2–9	NMRI: Feb. 24–26 ILTS: Feb. 4–11
Visible instruments	AVHRR	AVHRR AVNIR: Jan.–Mar.	AVHRR
Microwave instruments	SSM/I	SSM/I	SSM/I

NMRI: National Maritime Research Institute
ILTS: Institute of Low Temperature Science, Hokkaido University

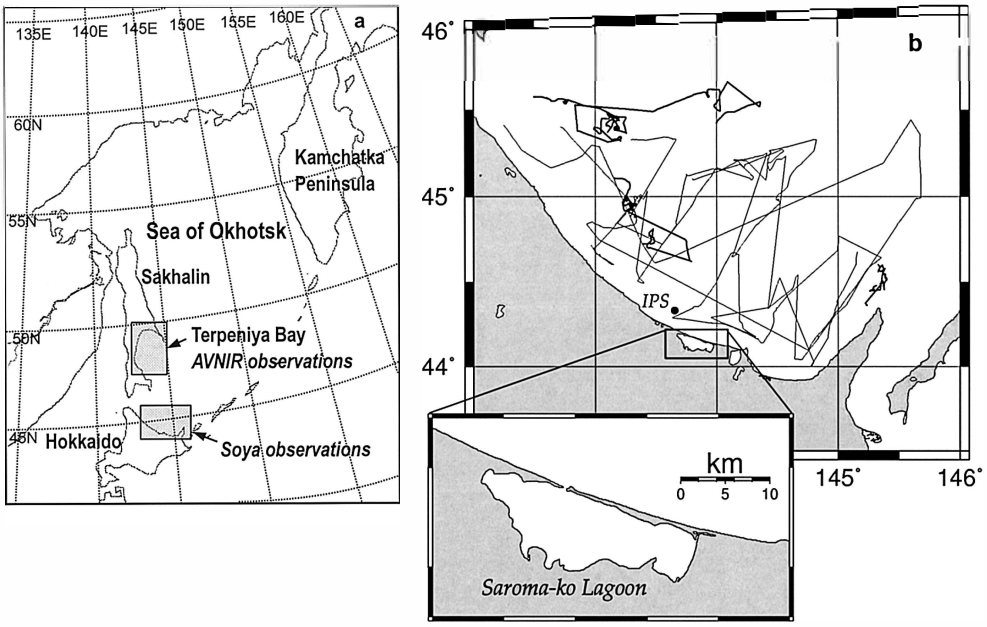

Fig. 1. The locations of the study area in the Sea of Okhotsk.
(a) The area of the icebreaker Soya observations and Advanced Visible and Near Infrared Radiometer (AVNIR) observations.
(b) The positions of ice thickness observations with ship tracks during 1996–1998 in the southernmost Sea of Okhotsk. Thin solid lines and thick solid lines mean operations by Institute of Low Temperature Science (ILTS), Hokkaido University and National Maritime Research Institute (NMRI), respectively. IPS with a black dot means the location of Ice Profiling Sonar observation in 1999. Saroma-ko Lagoon, where Airborne Microwave Radiometer observation was carried out in 1996, is indicated.

manual by measuring ice thickness from video images is less than a few centimeters at maximum (Shimoda *et al*., 1993; Toyota *et al*., 1999). Finally, the total number of observing days was 31 days for both sets of ice thickness observations.

Histograms of these ice thicknesses observed by the ILTS and the NMRI are shown in Fig. 2. These figures showed that sea ice from 20 cm to 60 cm in thickness was dominant in the southernmost Sea of Okhotsk in this period. On the other hand, the number of observed ice thicknesses data over 80 cm was few, because the sea ice thickness measurements by ship were carried out for single floes, not for ridged, rafted or hummocked ice floes. This bias on the ice thickness observation, originated in limitations of the ship's ice breaking ability and the measuring ability of the video imaging method, were considered. Ship tracks in Fig. 1b showed that the *Soya* did not tend to traverse along easy paths such as thin ice, cracks, leads or open water. Since the *Soya* has assigned inspectional and hydrographic missions, the *Soya* keeps to a route ice floes below one meter, which is the maximum ice thickness that can be broken by the *Soya*. Toyota and Kawamura (2002) validated their video imaging method by comparing with observations using the Ice-Profiling Sonar (IPS) during the winter of 1999. The result from these two methods shows good agreement in the ice thickness data below one meter. From IPS data, the ice thickness data over one meter were 8.4% of

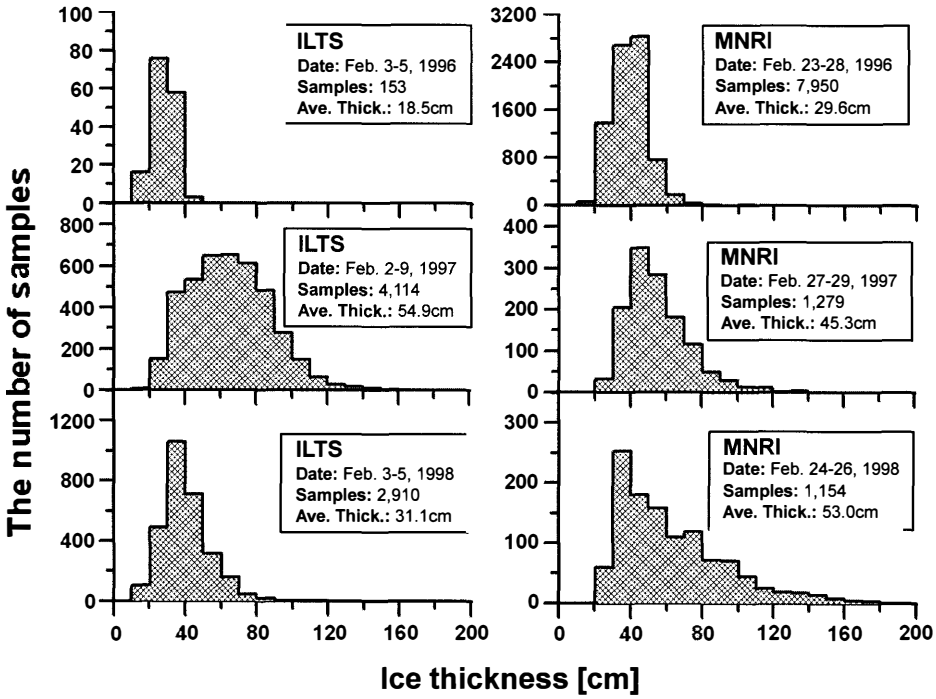

Fig. 2. Histograms of in-situ sea ice thicknesses observed by the Institute of Low Temperature Science (ILTS), Hokkaido University and National Maritime Research Institute (NMRI). Bin size is 10 cm. Date, the number of samples and average ice thickness are indicated in each figure.

the total, so that the contribution of thick ice above one meter seems to be small. Therefore the video imaging method can be considered as representative enough for the natural sea ice thickness distribution in the southern part of the Sea of Okhotsk.

Thin ice thickness data below 10 cm could not be observed because the video imaging method is valid only for hard and thick enough sea ice to have broken sides that will show up clearly in the observations. Therefore we employed visible images for thin ice thickness data in order to improve the accuracy of the ice thickness estimation for thinner ice below 10 cm.

2.1.2. Visible and near-infrared satellite image

Daily visible composite images from the Advanced Very High Resolution Radiometer (AVHRR) mounted on the National Oceanic and Atmospheric Administration (NOAA) satellites were used for checking cloud cover on ice and validating large-scale sea ice type samples for comparing with microwave observation and ship observations. The AVHRR has five channels ranging from 0.58 μm to 12.5 μm with a 1.1 km spatial resolution. We used 31 images, corresponding to the ship observations, of AVHRR received by Kitami Institute of Technology and compounded the images of ch. 1 (0.58–0.68 μm) and ch. 2 (0.725–1.10 μm).

The visible and near-infrared composite images, which were observed by the Advanced Visible and Near Infrared Radiometer (AVNIR) mounted on the Advanced Earth Observation Satellite (ADEOS), were also used for manual distinction of the newly formed "nilas" sea ice, which is below 10 cm thick, because the spatial resolution of AVHRR is not fine enough to distinguish nilas. The AVNIR data were obtained from the Earth Observation Research Center (EORC), National Space Development Agency of Japan (NASDA). The images were used during January–March 1997, because AVNIR was in use from August 1996 to June 1997. 11 AVNIR images were selected from around Terpeniya Bay, Sakhalin, where there is a large nilas area ($>20000\,km^2$), which appears stably for several months in winter, as shown in Fig. 1a. AVNIR has four channels ranging from 0.42 μm to 0.89 μm with a 16 m spatial resolution.

The composite images of ch. 1 (0.42–0.50 μm), ch. 2 (0.52–0.60 μm) and ch. 4 (0.76–0.89 μm) were used for identifying nilas from its surface features in this study. According to the sea ice type definition by the World Meteorological Organization (WMO, 1970), nilas is defined as a mat surface and thin elastic crust of ice, easily bending on waves and forming an interlocking pattern called "fingers" under swelling pressure. Owing to the existence of these distinctive features on the surface, it was easy to interpret whether an area was covered with nilas or not by AVNIR. Normally the thickness of newly formed ice is estimated from a satellite visible image by calculating the albedo. In this study, the area of nilas was determined manually only from ice surface features since the albedo conversion formula has not been obtained from AVNIR data yet. Nilas is up to 10 cm thick and can be subdivided into dark nilas (<5 cm thick) and light nilas (5–10 cm thick). For this study, the sea ice thickness is taken to be a constant thickness of 7 cm for sea ice, which is regarded as nilas detected by an AVNIR image. This value was determined for relatively uniform nilas in the range of 7 cm $\pm$ 2 cm by *in-situ* ship measurements off Mombetsu in the Sea of Okhotsk (unpublished data, 2001).

2.2. *Microwave data*

We used the daily brightness temperatures of the Special Sensor Microwave/Imager (SSM/I), which is a passive microwave radiometer mounted on the Defense Meteorological Satellite Program (DMSP) satellite. SSM/I data set is processed and provided by the National Snow and Ice Data Center (NSIDC), Colorado, U.S.A. The SSM/I has 7 channels, consisting of vertically and horizontally polarized 19 GHz, 37 GHz, 85 GHz channels and a vertically polarized 22 GHz channel. The spatial resolutions of 19 GHz, 22 GHz and 37 GHz channels are $25 \times 25\,km^2$. 85 GHz channels have a finer resolution ($12.5 \times 12.5\,km^2$) than the other channels. The 42 days data of SSM/I were compared with 31 days data for the ship observations in the southern part of the Sea of Okhotsk and 11 days data for the AVNIR images in Terpeniya Bay. Details of these collecting and comparing processes are presented in the next section.

2.3. *Data matching*

We used only 100% ice concentration samples, which were calculated by the NASA team thin ice algorithm, in order to avoid uncertainty of ice type classification and confusion with mixtures of thick ice and open water. However, the measured ice concentration is not that of just one ice type but is the sum of the ice concentrations of different ice types as described in Section 3.2. We obtained 75 ice thickness data for coupling with SSM/I from ship observations. The numbers of coupled ice thickness data varied from 5 to 194 samples of ship data, with one grid cell of SSM/I data coupled with 62 samples of ship data on average. The standard deviations of ship-SSM/I coupled data ranged from 3 cm to 26 cm and increased as the thickness of coupled data thickened.

In-situ ice thickness data and microwave data in different temporal and spatial scales were coupled. The video imaging method permits manual measurement of the thickness of each individual ice floe once in ten seconds at the maximum if the operator is capable of doing it. The sampling rate of this method depends on ice condition, so that the more the ice area is sparse, the more the sampling rate decreases. Hence ship observation provides ice thickness having temporal and spatial scales of once in several tens of seconds and several tens of meters, respectively, for about 10 hours continuously from early morning to evening. On the other hand, SSM/I observes sea ice in the Sea of Okhotsk for a short period in the morning and night in a day (ascending and descending). In this study, SSM/I data are daily means averaged from morning and night observations by NSIDC. The spatial resolution of SSM/I is $12.5 \times 12.5\,km^2$ at 85 GHz channels. According to Kimura and Wakatsuchi (2000), who analyzed sea ice motion on a $100 \times 100\,km^2$ scale, the maximum speed of ice drift is assumed to be 17 km/day in the Sea of Okhotsk, therefore the covering area of the SSM/I observation can be regarded as nearly the same as that of the ship observation for the same day.

Finally, we obtained 108 sea ice thicknesses from ground truth coupled with brightness temperatures from SSM/I, including 75 ship-SSM/I coupled data and the 33 AVNIR-SSM/I coupled data, as shown in Fig. 3. Ship-SSM/I coupled data ranged from about 20 cm to 85 cm after matching to the SSM/I polar stereographic grids. AVNIR-SSM/I coupled data were fixed to be 7 cm thick. The next section compares

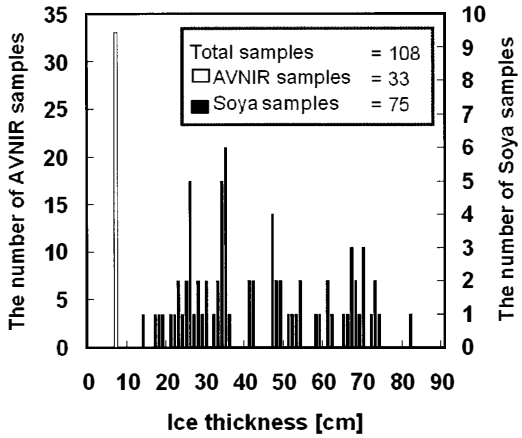

Fig. 3. Histograms of in-situ sea ice thickness data coupled of the brightness temperatures from SSM/I. These data consist of 75 ship-SSM/I coupled data with black bars and 33 AVNIR-SSM/I coupled data with a white bar.

these ice thickness data with ice classification parameters for estimating ice thickness.

3. Sea ice classification parameter

3.1. Sea ice classification

The WMO sea-ice nomenclature (1970) defined sea ice types, which reflected the age of the ice and thicknesses and different forms of ice at various stages of development. The ice types discussed in this study are limited to seasonal ice such as new ice (NEW), young ice (YOUNG) and first-year ice (FY). Those ice thickness ranges are defined by the WMO (1970) as $\leqq$10 cm, 11–30 cm, and $\geqq$31 cm, respectively. NEW is recently formed thin ice with no snow cover, represented generally by nilas, and includes frazil ice, grease ice, pancake ice, slush and shuga. YOUNG is also with no snow cover in the intermediate stage between NEW and FY. NEW and YOUNG can be regarded as having a wet surface due to the existence of a surface brine layer supplied through brine channels. FY is relatively dry, covered by snow, and is subdivided into thin first-year ice (31–70 cm thick), medium first-year ice (71–120 cm) and thick first-year ice (over 120 cm) in the Arctic and Antarctic. In this study, we used the thickness ranges as FY (31–80 cm) and Fast ice (81–120 cm), which is thicker and has more snow cover than FY, for the Sea of Okhotsk, based on field observations. The sizes of ice types are in proportion to their thicknesses except for nilas, due to ocean waves, because nilas is formed and maintained in calm water.

3.2. Polarization ratio

Cavalieri (1994) developed a sea ice classification parameter called the Polarization Ratio (*PR*) in the NASA team thin ice algorithm for the seasonal ice covered area. The PR is defined in terms of the brightness temperatures (T_B) obtained from 19 GHz horizontal (T_{B19H}) and vertical (T_{B19V}) polarization channels by the following equation.

$$PR = [T_{B19V} - T_{B19H}] / [T_{B19V} + T_{B19H}]. \quad (1)$$

PR values reflect the difference between vertical and horizontal polarizations of the same frequency and are mainly sensitive to ice surface characteristics such as roughness in the seasonally covered area. PR is not only a good water/ice discriminator, but is also largely independent of the physical temperature from the radiating medium since it is a ratio of observed radiances. PR is used to classify NEW, YOUNG and FY with limitation to the seasonal sea ice zone by using the physical characteristic that PR decreases with thickening of sea ice (Wensnahan *et al*., 1993; Cavalieri, 1994). The threshold values of PR for three ice types in the Bering Sea ranged from 0.11 to 0.17, 0.05 to 0.11 and 0.02 to 0.05 corresponding to NEW, YOUNG and FY, respectively, when ice concentration is 100%. According to Cavalieri (1994), these thresholds are in reasonable agreement with several sets of field observations, even if the exact range of PR for each ice type isuncertain. Martin *et al.* (1998) and Kimura and Wakatsuchi (1999) improved the validity of the ice classification using PR in the Sea of Okhotsk for detecting new ice production or polynyas, but these studies did not show exact values of thresholds for NEW, YOUNG and FY. Martin *et al.* (1998) used two ice types, FY and thin ice (TN), which were separated by the middle point (PR = 0.08 when ice concentration is 100%) between FY and TN. Kimura and Wakatsuchi (1999) classified NEW, YOUNG and FYdealing with PR as a continuous factor from NEW to FY. They set a threshold PR value between NEW and FY as well as the threshold value of Martin *et al.* (1998). These threshold values are compared with the *in-situ* ice thickness in Section 4.

3.3. *The ratio between T_{B37V} and T_{B85V} ($R_{37V/85V}$)*

According to Tateyama *et al.* (2000) and Nakayama *et al.* (2000), the vertically polarized channels of SSM/I showed that the dynamic range of the brightness temperature for snow covered thick sea ice widens with increase of frequency. That is to say, the vertically polarized 85 GHz (85 V) channel, which has the highest frequency of all SSM/I channels, has the widest dynamic range for thick ice, so that this channel may be better at detecting sea ice thickness. In addition, 85 V has also the finest spatial resolution. Although the brightness temperature of 85 V (T_{B85V}) is sensitive to ice surface temperature, this channel cannot distinguish between water and ice. However, the brightness temperature of the vertically polarized 37 GHz (T_{B37V}) can differentiate between water and ice; furthermore, this channel is useful for measuring ice surface temperature. Thus, $R_{37V/85V}$, defined as the ratio between T_{B37V} and T_{B85V} of SSM/I, was employed as a high spatial resolution ice classification parameter, having the advantages of both 85 V and 37 V (Tateyama *et al*., 2000). $R_{37V/85V}$ is given by the following equation.

$$R_{37V/85V} = T_{B37V} / T_{B85V}. \quad (2)$$

$R_{37V/85V}$ values increase with thickness and were used for ice type classification, because the difference of the brightness temperatures of both frequencies will increase with thickness in case of snow covered thick sea ice. Figure 4 shows a schematic of the microwave radiation model for NEW, YOUNG and FY, and the distribution of brightness temperature observed by an Airborne Microwave Radiometer (AMR) in

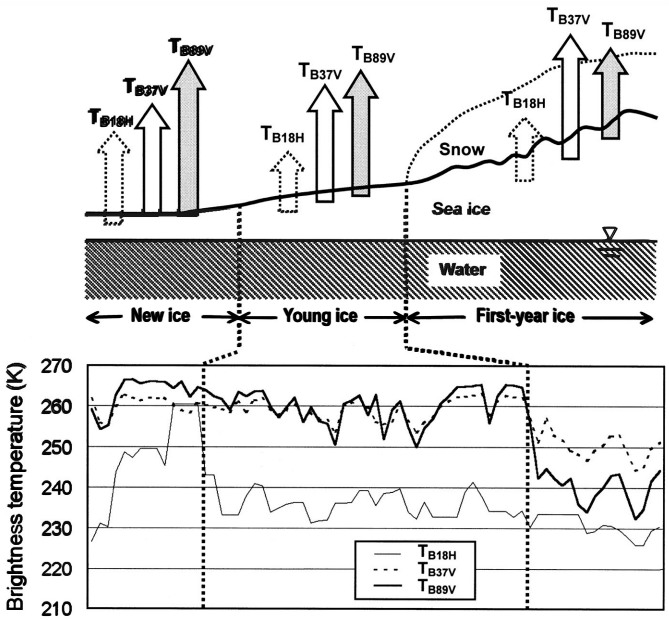

Fig. 4. A schematic of brightness temperature (T_B) radiation model on new ice, young ice and first-year ice and the distribution of brightness temperature observed by Airborne Microwave Radiometer in Saroma-ko Lagoon (Tateyama et al., 2000). The arrows on each ice type express the magnitude of microwave radiation and penetration depth for H-pol. 18 GHz (T_{B18H}), V-pol. 37 GHz (T_{B37V}) and V-pol. 89 GHz (T_{B89V}).

Saroma-ko Lagoon (Tateyama *et al.*, 2000) as shown in Fig. 1b. AMR has similar channels to SSM/I, for example, 18 GHz, 37 GHz and 89 GHz. The variability of SSM/I channels for these ice types was regarded as suitable for AMR channels in this study.

The surface of FY, which is over 30 cm thick and covered by snow, is relatively dry, because the brine drains with sea ice growth. The difference in emissivity between the vertically polarized 89 GHz (89 V) and 37 GHz (37 V) of AMR tends to be smaller with ice growth. For example, the difference between emissivities of 89 V and 37 V in NEW and FY are about 0.15 and 0.03, respectively (Eppler *et al.*, 1992). Therefore, the emissivity of 89 V can be regarded as the same as that of 37 V for FY. The penetration depths at 89 V and 37 V from FY become deeper than 5 mm and 18 mm, respectively, as sea ice thickens (Ulaby *et al.*, 1986). Generally, the physical ice temperature is warmer in deeper layers than that in the shallower layer due to cold air and snow insulation during the freezing season. The difference between physical temperatures at the snow-ice interface detected by 89 V and at the deeper layer detected by 37 V become larger with ice growth. In microwave radiometry, the observed T_B is expressed by the product of emissivity and physical temperature. The T_{B89V} is higher than T_{B37V} for NEW and YOUNG, while the reverse tendency is found for FY. The difference between T_{B89V} and T_{B37V} is more significant for FY than NEW and YOUNG. The rate of T_{B37V} to T_{B89V} reflects the difference of physical temperature at each channel's penetration depth and becomes larger when sea ice thickens. Therefore $R_{37V/89V}$ in-

creases with ice growth as shown in eq. (2).

YOUNG, which was defined as ice having no snow cover and a thickness of 11–30 cm, shows a slightly lower brightness temperature on 37 V of AMR than on 89 V except the case of a rapid decrease of 89 V where ice thickness changed from typical YOUNG to near FY as shown in Fig. 4. The penetration depths at 89 V and 37 V for YOUNG are 2 mm and 5 mm, respectively (Ulaby *et al*., 1986). In these shallow ice layers, the difference between physical temperatures of 89 V can be regard as same as that of 37 V. Therefore the difference between those brightness temperatures is dominated by the difference between emissivities of 89 V and 37 V, which is thought to be caused by brine in the surface layer. The absorption of the brightness temperature on 89 V by brine, which is liquid saline water, is greater than that on 37 V, and then 89 V tends to indicate a smaller value than 37 V in case of brine-rich thin ice.

On NEW, snow is blown away by wind or mixed into the high saline slush layer, so consequently the new ice surface is wet. It is difficult to distinguish new ice by using $R_{37V/89V}$, because microwaves will be emitted from a nearly ice surface at both frequencies, 89 GHz and 37 GHz. Even if $R_{37V/89V}$ calculated from NEW samples shows slightly smaller values than $R_{37V/89V}$ of YOUNG, it is not significant. On the other hand, the horizontal polarization channels of AMR indicated that the dynamic range of the brightness temperature for NEW widens with decrease of frequency. Therefore T_{B18H} (18H) of AMR is the most appropriate channel to detect NEW among the other channels as shown in Fig. 4. T_{B19H} (19 H) of SSM/I is also useful for detecting new ice (Nakayama *et al*., 2000). To identify NEW by SSM/I, $R_{19H/85V}$, which is the ratio between 19 H and 85 V, was defined (Tateyama *et al*., 2000). If $R_{19H/85V}$ ranged from 0.70 to 0.83, then $R_{19H/85V}$ values were converted to new $R_{37V/85V}$ by the following empirical formula,

$$R_{37V/85V} = 0.30 \cdot (*R_{37V/85V} - R_{19H/85V}) + 0.6 \cdot R_{19H/85V} + 0.29, \qquad (3)$$

where $*R_{37V/85V}$ is the value calculated from eq. (2). When a NEW signal is detected, $*R_{37V/85V}$ is converted to $R_{37V/85V}$ by eq. (3), keeping a linear relationship between this parameter and ice thickness. In case of YOUNG or FY, this process is skipped, so that $R_{37V/85V}$ is equal to $*R_{37V/85V}$.

4. Results

This section describes the relationship between ice classification parameters and ice thickness, which were collected from ground truth and were averaged into the SSM/I polar stereographic grids. Figure 5 is a plot of PR *vs. in-situ* ice thickness and shows that PR values were affected greatly by ice thickness. PR showed a linear relationship with *in-situ* ice thickness having a good correlation (-0.77). This result suggests that it is possible to use the ice classification parameter PR as an ice thickness indicator for sea ice in the Sea of Okhotsk in February. The threshold values ((a) in Fig. 5) of PR for NEW, YOUNG and FY were validated in the Bering Sea by Cavalieri (1994). Changing those values from 0.09 to 0.13, 0.07 to 0.09 and 0.03 to 0.07 for NEW, YOUNG and FY ((b) in Fig. 5), respectively, the ice types for the Sea of Okhotsk become closer to ones defined by the WMO sea-ice nomenclature. The overall accura-

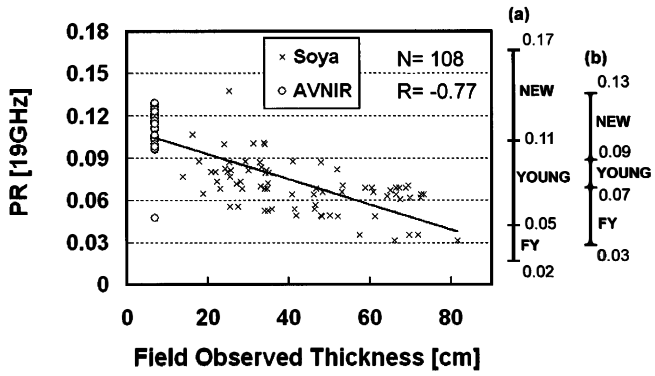

Fig. 5. The sensitivity test of Polarization Ratio (PR) to the in-situ ice thickness derived from Soya observations in Februaries 1996–1998, and AVNIR images in February–March 1997. N and R denote the number of samples and the correlation coefficient, respectively. The solid line means the linear regression between PR and Soya - AVNIR ice thickness data.

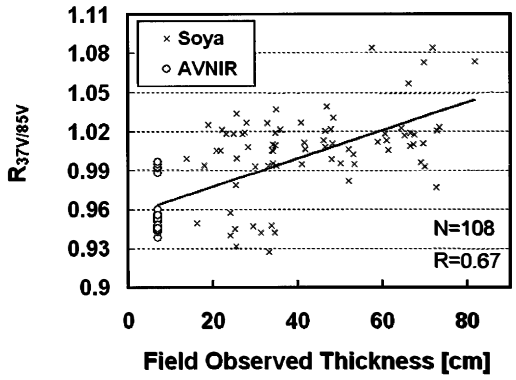

Fig. 6. The sensitivity test of the ratio between the brightness temperatures of 37 GHz and 85 GHz vertical polarization channels ($R_{37V/85V}$) to the in-situ ice thickness as well as Fig. 5. N and R denote the number of samples and the correlation coefficient, respectively. A solid line means the linear regression between PR and Soya-AVNIR ice thickness data.

cy of estimation of ice thickness by PR seems to be good, but the observed *in-situ* ice thickness varies widely for each ice type. To obtain a highly accurate ice thickness estimated from satellite microwave radiometer, it is necessary to separate completely signals from NEW and FY at least.

The parameter $R_{37V/85V}$ can be used to estimate the ice thickness as discussed in Section 3.3. Figure 6 shows a relation of $R_{37V/85V}$ to *in-situ* ice thickness. The correlation coefficient of $R_{37V/85V}$ with *in-situ* ice thickness was slightly lower ($R=0.67$). Although $R_{37V/85V}$ varied widely as a whole, the groups of NEW and FY can be more distinguished from PR. The relation between PR and $R_{37V/85V}$ for the ice types is shown in Fig. 7. It appears that $R_{37V/85V}$ can differentiate the ice types more than PR itself.

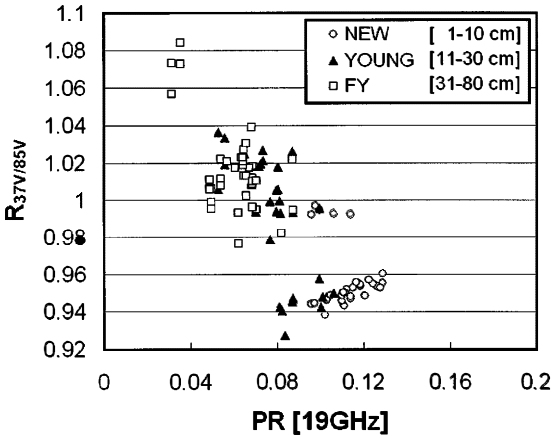

Fig. 7. Polarization Ratio (PR)—the ratio between the brightness temperatures of 37 GHz and 85 GHz vertical polarization channels ($R_{37V/85V}$). New ice (NEW), young ice (YOUNG) and first-year ice (FY) signals derived from Soya observation in Februaries 1996–1998, and AVNIR images in February–March 1997 are plotted.

Table 2. Thresholds of ice type and related ice thickness ranges for PR of the NASA team thin ice algorithm and $R_{37V/85V}$ of the S/KIT algorithm in the Sea of Okhotsk. NEW, YOUNG and FY mean new ice, young ice and first-year ice, respectively. The threshold values of PR^1 were defined by Cavalieri (1994) for the Bering Sea. The threshold values of PR^2, PR^3 and PR^4 were defined for the Sea of Okhotsk by Martin et al. (1998), Kimura and Wakatsuchi (1999), and this study, respectively. PR^4 and $R_{37V/85V}$ were derived from validation with in-situ ice thickness data.

	NEW	YOUNG	FY	Fast ice
Thickness	≤10 cm	11–30 cm	30–80 cm	≥81 cm
PR^1 (Cavalieri, 1994)	0.11–0.17	0.05–0.11	0.02–0.05	–
PR^2 (Martin *et al*., 1998)	0.08–0.13		0.03–0.08	–
PR^3 (Kimura and Wakatsuchi, 1999)	0.08–0.13		0.03–0.08	–
PR^4 (this study)	0.09–0.13	0.07–0.09	0.03–0.07	–
$R_{37V/85V}$	0.92–0.97	0.97–1.00	1.00–1.12	1.12–1.20

The correlation of PR and $R_{37V/85V}$ can improve separating the ice types. The relation of the ice thickness to PR and $R_{37V/85V}$ will be discussed in the next chapter.

The threshold values of PR and $R_{37V/85V}$ for the Sea of Okhotsk are summarized in Table 2, comparing with the threshold values investigated form past studies. The PR threshold values derived by Martin *et al.* (1998) and Kimura and Wakatsuchi (1999)

showed good agreement with the PR threshold values in this study. A large part of the difference between Cavalieri's PR threshold values and other PR threshold values for the Sea of Okhotsk is due to the difference of study area; the effect of other physical reasons such as the difference of snow depth or wetness is not clear.

5. Discussion

The abilities of PR and $R_{37V/85V}$ in the estimation of sea ice thickness were investigated. Multiple regression analysis using PR and $R_{37V/85V}$ was carried out to determine if the combination of parameters could provide a better estimate of ice thickness than a single one. This resulted in the following formula to estimate sea ice thickness H (cm).

$$H = -537.33 \cdot PR + 83.88 \cdot R_{37V/85V} - 6.91. \quad (4)$$

Figure 8 shows the correlation between the *in-situ* ice thickness and estimated ice thickness from eq. (4). The correlation coefficient of H and *in-situ* ice thickness showed agreement at a high statistical significance ($R = 0.81$), an increase over the -0.77 from PR alone, with the root mean square error being 14 cm. $R_{37V/85V}$ contributes positively to estimation of ice thickness owing to its ability to separate NEW and FY. It is found in Fig. 8 that the estimated ice thickness tends to be overestimated below 50 cm in *in-situ* ice thickness and to be underestimated above 50 cm thick. The overestimating problem below 50 cm was considered partly because of the existence of ridged or rafted ice which can be observed by SSM/I more frequently than by ship's video observation. This problem is expected to be solved by combining IPS data with *in-situ*

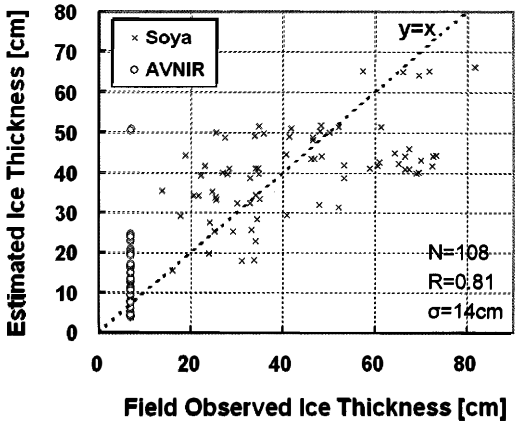

Fig. 8. The relationship between in-situ ice thickness and estimated ice thickness calculated by multiple regression analysis using Polarization Ratio (PR) and the ratio between the brightness temperatures of 37 GHz and 85 GHz vertical polarization channels ($R_{37V/85V}$). N, R and σ denote the number of samples, the correlation coefficient and root mean square error, respectively. The dashed line is the imaginary line $y = x$.

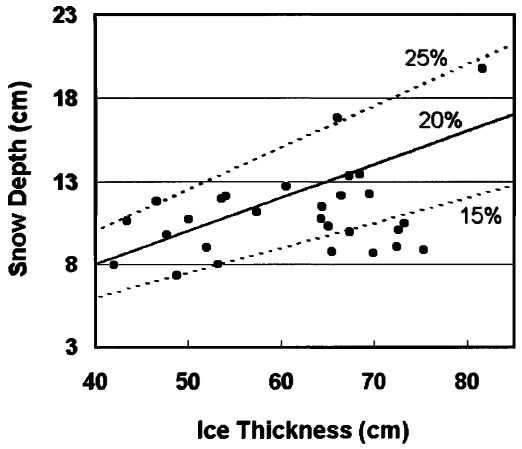

Fig. 9. The relationship between snow depth on sea ice and ice thickness from video observations by the Institute of Low Temperature Science, Hokkaido University on board the icebreaker Soya during 1996–1998. Imaginary lines, which mean snow depth corresponding to 15%, 20% and 25% of ice thickness, are indicated.

ice thickness data to supplement ship observations in future work.

One of the reasons for the underestimating problem in thicker ice is the snow cover effect. The effect of snow cover over sea ice on our estimation of ice thickness cannot be neglected, because 85 GHz is more sensitive to surface changes than the other SSM/I channels. Snow cover measurement was carried out by ILTS using a manual video imaging method in combination with thickness observations during 1996–1998. From this observation, it was found that the snow cover varied from 8 cm to 13 cm and did normally not exceed 20%±5% of the ice thickness in the large ice drifting region (Fig. 9). This result agrees with Perovich *et al.* (1988) who confirmed that the snow cover on FY never exceeded 20 cm and averaged 8 cm. Therefore, the snow cover effect on the estimation of ice thickness by satellite microwave radiometer generally can be regarded as a constant during the freezing season in the seasonal ice covered area. However, it was found that ice thicknesses underneath snow cover of less than 15% of the ice thickness were underestimated. The uncertainties associated with the snow cover are not explained by only the depth of snow, but also wetness, grain size and density of snow and surface brine on the snow-ice interface. Although we have no validation data of snow cover without snow depth, the snow effect except melting can be regarded as a constant in a large scale observation by satellite.

Flood and melt-water on the snow-ice interface affects the mixing ratio of constituent dielectrics and the dielectric roughness of the interface layer, thus may change the microwave signature, even if the snow cover is optically thin (Eppler *et al.*, 1992). In this study, a rapid increase of the ice thickness was found for a few days in the melting season detected from SSM/I data, when both 37 V and 85 V of SSM/I show a sharp increase. This rapid increase of ice thickness can be detected by monitoring daily air temperature and rapid changes in microwave data, and further errors of thickness can

be minimized by obtaining of correct values from microwave data.

Although there are still some problems about coupling *in-situ* ice thickness, the snow cover effect and the surface melting contamination, these results suggest that it is possible to infer sea ice thickness from satellite passive microwave data.

6. Summary

In-situ ice thickness data in the southern part of the Sea of Okhotsk have been derived from icebreaker *Soya* observations during 1996–1998. The video imaging method underestimates thickness above one meter and overestimates those below 10 cm by several parcent. We obtained 108 samples of *in-situ* sea ice thickness averaged onto SSM/I polar stereographic grids, including 75 thicker ice thickness data from on board *Soya*, and 33 thinner ice thickness data from AVNIR. We should take AVNIR data including the bias into account because we set the thickness of newly formed ice as a constant value, 7 cm thick.

The ice classification parameter PR of the NASA team thin ice algorithm was examined for its ability to estimate ice thickness using these validation data. PR showed high sensitivity for *in-situ* sea ice thickness with the correlation coefficient R being -0.77. A separator between new ice and first-year ice, $R_{37V/85V}$, was also applied to a comparison with *in-situ* sea ice thickness and showed a slightly lower correlation coefficient $R=0.67$ than that of PR.

A formula to estimate sea ice thickness from PR and $R_{37V/85V}$ was derived empirically and showed a good correlation ($R=0.81$) with the root mean square error being 14 cm. These results in the southern Sea of Okhotsk suggest that it is possible to assume sea ice thickness from satellite microwave data. It is necessary to continue the comparison with the brightness temperature data observed by the satellite microwave radiometer and accumulated ship observation data or other *in-situ* ice thickness data including ridged or rafted sea ice. Further studies are also needed to research the relationships between observed microwave radiation and sea ice thickness affected by snow cover and surface melting.

Acknowledgments

We used AMR data and ADEOS AVNIR images provided by the National Space Development Agency of Japan (NASDA). SSM/I polar stereographic grid data were obtained from the National Snow and Ice Data Center (NSIDC) in Boulder, Colorado by CD-ROM and via the World Wide Web. We would like to thank the Institute of Low Temperature Science, at Hokkaido University and the National Maritime Research Institute for supplying us with ice thickness data measured by the icebreaker *Soya*. We are also thankful for the help of the *Soya* crews of the Japan Coast Guard.

This study was partly supported by NASDA through the Arctic Research program using the IARC (International Arctic Research Center)-NASDA Information System (PI. Enomoto).

References

Cavalieri, D.J. (1994): A microwave technique for mapping thin ice. J. Geophys. Res., **99**, 12561–12572.

Cavalieri, D.J., Gloersen, P. and Campbell, W.J. (1984): Determination of sea ice parameters with the NIMBUS 7 SMMR. J. Geophys. Res., **89**, 5355–5369.

Comiso, J.C. (1995): SSM/I ice concentration using the Bootstrap algorithm. NASA Tech. Rep, **1380**, 50p.

Eppler, D.T., Farmer, L.D., Lohanick, A.W., Anderson, M.R., Cavalieri, D.J., Comiso, J., Gloersen, P., Garrity, C., Grenfell, T.C., Hallikainen, M., Maslanik, J.A., Matzler, C., Melloh, R.A., Rubinstein, I. and Swift, C.T. (1992): Passive microwave signatures of sea ice. Microwave Remote Sensing of Sea Ice, ed. by F. Carsey. Washington, D.C., Am Geophys. Union, 47–71 (Geophys. Monogr. Ser., **68**).

Grenfell, T.C. and Comiso, J.C. (1986): Multifrequency passive microwave observations of first-year sea ice grown in a tank. IEEE Trans. Geosci. Remote Sensing, **24**, 826–831.

Grenfell, T.C., Cavalieri, D.J., Comiso, J.C., Drinkwater, M.R., Onstott, R.G., Rubinstein, I., Steffen, K. and Winebrenner, D.P. (1992): Considerations for microwave remote sensing of thin sea ice, Microwave Remote Sensing of Sea Ice, ed. by F. Carsey. Washington, D.C., Am Geophys. Union, 291–301 (Geophys. Monogr. Ser., **68**).

Haas, C. (1997): Comparison of sea-ice thickness measurements under summer and winter conditions in the Arctic using a small electromagnetic induction device. Geophysics, **62**, 749–757.

Ishizu, M., Mizutani, K. and Itabe T. (1999): Airborne freeboard measurements of sea ice and lake ice at the Sea of Okhotsk coast in 1993–95 by a laser altimeter. Int. J. Remote Sensing, **20**, 2461–2476.

Kimura, N. and Wakatsuchi, M. (1999): Processes controlling the advance and retreat of sea ice in the Sea of Okhotsk. J. Geophys. Res., **104**, 11137–11150.

Kimura, N. and Wakatsuchi, M. (2000): Relationship between sea-ice motion and geostrophic wind in the Northern Hemisphere. Geophys. Res. Lett., **27**, 3735–3738.

Martin, S., Drucker, R. and Yamashita, K. (1998): The production of ice and dense shelf water in the Okhotsk Sea polynyas. J. Geophys. Res., **103**, 27771–27782.

Multala, J., Hautaniemi, H., Oksama, M., Leppäranta, M., Haapala, J., Herlevi, A., Riska, K. and Lensu, M. (1996): An airborne electromagnetic system on a fixed wing aircraft for sea ice thickness mapping. Cold Reg. Sci. Technol., **24**, 353–373.

Nakayama, M., Cho, K., Shimoda, H., Sakata, T., Tanikawa, T. and Nishio, F. (2000): Evaluation of frequency band and polarization of microwave radiometer for observation of first-year ice in the Okhotsk Sea. Seppyo (J. Jpn. Soc. Snow Ice), **62**, 523–535 (in Japanese with English abstract).

Perovich, D.K., Gow, A.J. and Tucker III, W.B. (1988): Physical properties of snow and ice in the winter marginal ice zone of Fram Strait. Proceedings of the IGARS '88 Symposium, Scotland, European Space Agency, **ESA SP-284**, 1119–1123.

Rothrock, D.A., Yu, Y. and Maykut, G.A. (1999): Thinning of the Arctic sea-ice cover. Geophys. Res. Lett., **26**, 3469–3472.

Shimoda, H., Endo, T., Muramoto, K., Ono, N., Takizawa, T., Ushio, S., Kawamura, T. and Oshima, K. (1997): Observations of sea-ice conditions in the Antarctic coastal region using ship-boad video cameras. Nankyoku Shiryô (Antarct. Rec.), **41**, 355–365 (in Japanese with English abstract).

Tateyama, K., Enomoto, H., Takahashi, S., Shirasaki, K., Hyakutake, K. and Nishio, F. (2000): New passive microwave remote sensing technique for sea ice in the Sea of Okhotsk using 85-GHz channel of DMSP SSM/I. Bull. Glaciol. Res., **17**, 23–30.

Toyota, T. and Kawamura, T. (2002): Sea ice properties in the coastal region of the Sea of Okhotsk off Hokkaido. Gekkan Kaiyo (Kaiyo Monthly), **Gogai 30**, 32–44 (in Japanese).

Toyota, T., Ukita, J., Ohshima, K.I., Wakatsuchi, M. and Muramoto, K. (1999): A measurement of sea ice albedo over the southwestern Okhotsk Sea. J. Meteorol. Soc. Jpn., **77**, 117–133.

Ukita, J., Kawamura, T., Tanaka, N., Toyota, T. and Wakatsuchi, M. (2000): Physical and stable isotopic properties and growth processes of sea ice collected in southern Sea of Okhotsk. J. Geophys. Res., **105**, 22083–22093.

Ulaby, F.T., Moore, R.K. and Fung, A.K. (1986): Microwave Remote Sensing—Active and Passive, **Vol. III**: From Theory to Applications. Dedham, Artech House, 1120 p.

Wadhams, P. (1997): Ice thickness in the Arctic Ocean: The statistical reliability of experimental data. J. Geophys. Res., **102**, 27951–27959.

Wadhams, P., Davis, N.R., Comiso, J.C., Kutz, R., Crawford, J., Jackson, G., Krabill, W., Sear, C.B., Swift, R. and Tucker III, W.B. (1991): Concurrent remote sensing of arctic sea ice from submarine and aircraft. Int. J. Remote Sensing, **12**, 1829–1840.

Wensnahan, M., Maykut, G.A. and Grenfell, T.C. (1993): Passive microwave remote sensing of thin sea ice using principal component analysis. J. Geophys. Res., **98**, 12453–12468.

World Meteorological Organization (1970): WMO sea-ice nomenclature, terminology, codes and illustrated glossary. Geneva, World Meteorological Organization, WMO/OMM/BMO-**259**, TP. 145.

(Received January 29; Revised manuscript accepted July 25, 2002)